PROCEEDINGS, 51st Workshop on Geothermal Reservoir Engineering
Stanford University, Stanford, California, February 9-11, 2026
SGP-TR-230

Microseismic Location in EGS: Comparing picking-based and source-imaging workflows on downhole DAS data

Xiaoming Zhang[1], Eyal Shimony[2], Junhao Song[3], Uri Wygodny[2], Weiqiang Zhu[3], Ariel Lellouch[2], Noam Zach Dvory[1,4]

[1]Energy and Geoscience Institute, University of Utah, Salt Lake City, UT, USA

[2]School of the Environment and Earth Sciences, Tel Aviv University, Israel

[3]Department of Earth & Planetary Science, University of California, Berkeley, USA

[4]Department of Civil and Environmental Engineering, University of Utah, Salt Lake City, UT, USA

Xiaoming.Zhang@utah.edu

nzd@egi.utah.edu

Keywords: Enhanced Geothermal Systems, Induced seismicity, Microseismic monitoring, Distributed acoustic sensing, Phase picking, Source imaging

ABSTRACT

Accurate microseismic locations are essential for developing and monitoring enhanced geothermal systems (EGS). Joint use of downhole geophones and distributed acoustic sensing (DAS) can boost detection and location performance, but conventional picking-based workflows perform sub-optimally on DAS data because individual channels are noisy. In addition, DAS's unidirectional measurements create blind spots that depend on the acquisition geometry, source location, focal mechanism, and subsurface structure. We compare a traditional, picking-based locator with a picking-free source-imaging workflow that jointly exploits P- and S-wave phases on DAS and geophones. The source-imaging method applies an STA/LTA transform to enhance P-wave coherence and mitigate blind spots due to DAS directivity. Our analysis clarifies the strengths and downsides of each approach and shows that combining them improves catalog completeness and location accuracy and resolution, with specific benefits for real-time detection of shear onset and runaway slip. These results inform real-time monitoring, risk assessment, and stimulation planning in EGS operations.

1. INTRODUCTION

Accurate and timely microseismic catalogs are essential for understanding fracture development, reservoir stimulation processes, and seismic hazard during enhanced geothermal system (EGS) operations (Folesky et al., 2016; Majer et al., 2007; Moore et al., 2019; Xiaoming & Dvory, 2026). High-resolution event detection and location enable operators to track the evolution of induced seismicity in near real time, providing critical information for stimulation optimization and risk mitigation (Perol et al., 2026; Stewart, 1977). As EGS projects increasingly rely on dense monitoring arrays, the resulting data volumes demand robust and computationally efficient processing workflows capable of operating under challenging signal-to-noise conditions.

In recent years, distributed acoustic sensing (DAS) has emerged as a powerful complement to conventional downhole geophones, offering dense spatial sampling along boreholes and improved sensitivity to small-magnitude events (Daley et al., 2013; Zhan, 2019). However, DAS measurements are inherently directional and often noisier on a channel-by-channel basis, which can degrade the performance of traditional phase picking and location methods. Blind spots associated with DAS directivity further complicate event detection and location, particularly when acquisition geometry, focal mechanism, and subsurface structure are unfavorable.

Picking-based workflows, especially those leveraging deep-learning phase pickers, have demonstrated strong performance for induced seismicity monitoring. When combined with sequential association and location algorithms, such approaches can efficiently generate high-quality event catalogs from large datasets, e.g., LOC-FLOW (Zhang et al., 2022). At the Utah FORGE site, deep-learning-based pick-driven workflows have been successfully applied to near-surface seismic arrays (Niemz et al., 2025). In this study, we extend this approach to downhole monitoring data acquired during the 2024 Utah FORGE stimulation, consisting of one DAS cable and two co-located geophone strings. The resulting catalog exhibits spatial patterns consistent with an existing reference catalog (hereafter referred to as the GES (Geo Energy Suisse) catalog (Dyer et al., 2024)), despite differences in processing methodology.

As an alternative to picking-based approaches, waveform-based source imaging methods provide a picking-free means of locating seismic sources. The Source-Scanning Algorithm (SSA) (Kao & Shan, 2004) maps the spatial and temporal distribution of seismic energy by evaluating waveform coherency across an array for a range of trial source locations and origin times. By exploiting full waveform information rather than discrete phase picks, SSA is inherently robust to high noise levels and does not require assumptions about fault geometry or rupture orientation. This makes it particularly attractive for DAS applications, where dense spatial sampling can be leveraged to enhance imaging performance despite individual-channel noise and directional sensitivity.

In this study, potential fault structures were identified by analyzing the spatial and temporal clustering of microseismic events using a Python-based workflow (Zhang et al., 2025; Zhang & Dvory, 2025). This workflow was applied to compare three microseismic catalogs: (1) a catalog generated using the picking-based location method, (2) a catalog generated using the source-scanning (SSA) method, and (3) the reference GES catalog (Dyer et al., 2024). The comparison enables an assessment of how differences in detection and location methodologies influence the inferred fault geometry and seismicity patterns, providing further insight into the strengths and limitations of each catalog for characterizing stimulation-induced fracture development.

2. STUDY SITE

The Utah Frontier Observatory for Research in Geothermal Energy (FORGE) (Moore et al., 2019) is a dedicated enhanced geothermal system (EGS) research site located near Milford, Utah, within the Mineral Mountains region. The site was established by the U.S. Department of Energy as a field laboratory for developing, testing, and validating technologies to advance EGS deployment. Utah FORGE is characterized by high geothermal gradients, crystalline basement rocks, and low natural permeability, making it well-suited for controlled stimulation experiments and induced seismicity studies.

Multiple hydraulic stimulation campaigns have been conducted at the site to enhance reservoir permeability through shear stimulation of pre-existing fracture (Dyer et al., 2022, 2024; England, 2024; McLennan, 2022). These operations are accompanied by a comprehensive seismic monitoring network, including near-surface stations, downhole geophones, and distributed acoustic sensing (DAS) deployed along monitoring wells. The dense instrumentation provides high-resolution observations of induced microseismicity, enabling detailed analyses of fracture activation, fault development, and seismic hazard.

The data analyzed in this study were acquired during the April 2024 stimulation experiments, which targeted different reservoir intervals and injection strategies. These datasets offer an opportunity to evaluate and compare microseismic detection and location workflows under varying operational conditions, while leveraging a well-characterized geological and monitoring environment.

3. METHODOLOGY

3.1 Phase-Picking Event Location Method

The PhaseNet model (Zhu & Beroza, 2019) has been used to perform P and S phase picking on seismic data collected by downhole geophones installed at well 56 and 78B and downhole DAS along the production well 16B. Compared with three-component geophone sensors, individual DAS channels have only the uniaxial component along the fiber, resulting in noisier seismic recordings. In comparison, microseismic signals are more readily observed in geophone recordings. Here, we first used geophone picks for event detection, then included DAS picks to further refine the location. The workflow is designed in detail below:

1. We first used the GaMMA algorithm (Zhu et al., 2025) to associate phase arrivals with individual microseismic events.
2. We selected 2948 events that are also well recorded by the downhole DAS (i.e., picks reported by at least half of the DAS channels) to further improve their locations.
3. We used the ADLoc algorithm (Zhu et al., 2025) to locate each event by repeating the location process 200 times and resampling 90% of the downhole geophone and DAS picks each time. The location with the highest probability is selected as the final event location, and the standard deviation of the locations along each axis is taken as uncertainty.
4. A local magnitude formulation based on the GES catalog magnitude and the measured maximum strain rate along the DAS has been derived and then applied to all the events in our catalog.

The uniform velocity model, which was used during real-time monitoring (i.e., used for the GES catalog), has been adopted in the above association and location steps. Note that including near-source DAS picks has greatly improved the locations, as it's challenging to achieve robust locations with 2 downhole geophones due to geometry ambiguity.

3.2 Waveform-Based Source Imaging Method

The 2024 dataset included an expanded 24-channel geophone array installed in borehole 78B-32 (depth 1465–1678 m from wellhead) and a high-resolution DAS array deployed in borehole 16B(78)-32 (depth 1600-2492 m from wellhead), composed of 1496 channels. The P- and S-wave velocity model assumed a constant velocity below the granitic contact at approximately 905 m depth. Both datasets were acquired at a sampling rate of 4000 Hz with a 12s recording duration. The DAS data were stored in SEGY format, and the geophone data in miniSEED format.

The raw waveform gathers were transformed into Short-Term Average/Long-Term Average (STA/LTA) characteristic functions. This transformation is critical for facilitating the integration of the DAS and inertial geophone arrays, while simultaneously mitigating the geometric constraints inherent to DAS, such as polarity reversals and P-wave shadow zones.

By converting raw strain into a positive energy ratio, the algorithm resolves polarity ambiguities and normalizes amplitudes. This normalization prevents high-amplitude S-waves from disproportionately dominating the stack, ensuring that weaker P-wave onsets, even those arriving orthogonal to the fiber axis, contribute coherently to the final brightness function. Furthermore, to address the vertical fiber's azimuthal ambiguity, the acquisition system was organized into two complementary subarrays. Crucially, the integration of the three-component geophones breaks the cylindrical symmetry of the DAS data, enabling highly focused source localization.

To determine the event's origin, a 1 [km] square search grid with a 40 [m] spatial resolution was used as the 3D source location, as shown in Figure 1. Utilizing the known receiver geometry and an isotropic velocity model, theoretical travel times are computed via an Eikonal ray-tracing solver. These travel times are then used to time-shift the traces to a common reference time.

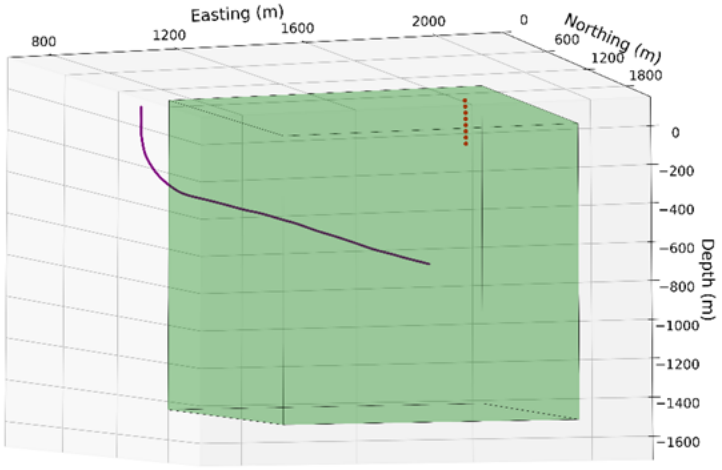

Figure 1: Three-dimensional view of the geometry layout. The setup includes the DAS fiber trajectory (purple) and the borehole geophone array (red). The green box outlines the search grid volume.

For each waveform receiver, a partial brightness sum was calculated as:

$$s_j^{(P|S)}(t;\eta) = \frac{1}{L_j}\sum_{i=1}^{N_j} \mathrm{STA/LTA}\left(u_i^j\left(t + \tau_{\eta r_i}^{(P|S)}\right)\right) \tag{1}$$

The total brightness function is defined as:

$$\mathrm{br}(\eta) = A\sum_{j=1}^{N_j} s_j^P\left(t_j^P\right) + s_j^S\left(t_j^S\right) - \sigma\left(\left\{t_j^P, t_j^S \middle| 1 \le j \le N_j\right\}\right) - \left(t_{\mathrm{DAS}}^{\mathrm{P}} - t_{\mathrm{DAS}}^{\mathrm{S}}\right) \tag{2}$$

Where the first term is the score received from the partial brightness sum that flattened the gather. All the other terms in the equation penalize the score by addressing the median absolute deviation, the standard deviation score, and DAS's discrepancies between P and S phases. The resulting brightness field is converted into a PDF to provide probabilistic event locations and quantify uncertainty. The final event location is determined as the geometric median of the PDF, using a probability threshold of 0.03 to isolate the high-confidence region. To improve event positioning, several V_p/V_s ratios were tested, and the optimal ratio was selected as the one that maximized the summed brightness across a subset of reference events.

4. RESULTS

4.1 Microseismic Catalog from Phase-Picking

We have derived a catalog of 2948 well-recorded microseismic events using the deep-learning picks-based workflow. We compared our catalog with the GES catalog, and their spatial distributions in general agree well with each other. In our catalog, the fracture zones have been clearly identified and show similar strike and length scales. However, the lateral extent of the western part shows a different pattern, with two near-linear branches merging near the DAS cable (production well). It's still unclear whether this is due to artifacts from the limitations of our current workflow or to the structures of realistic fractures.

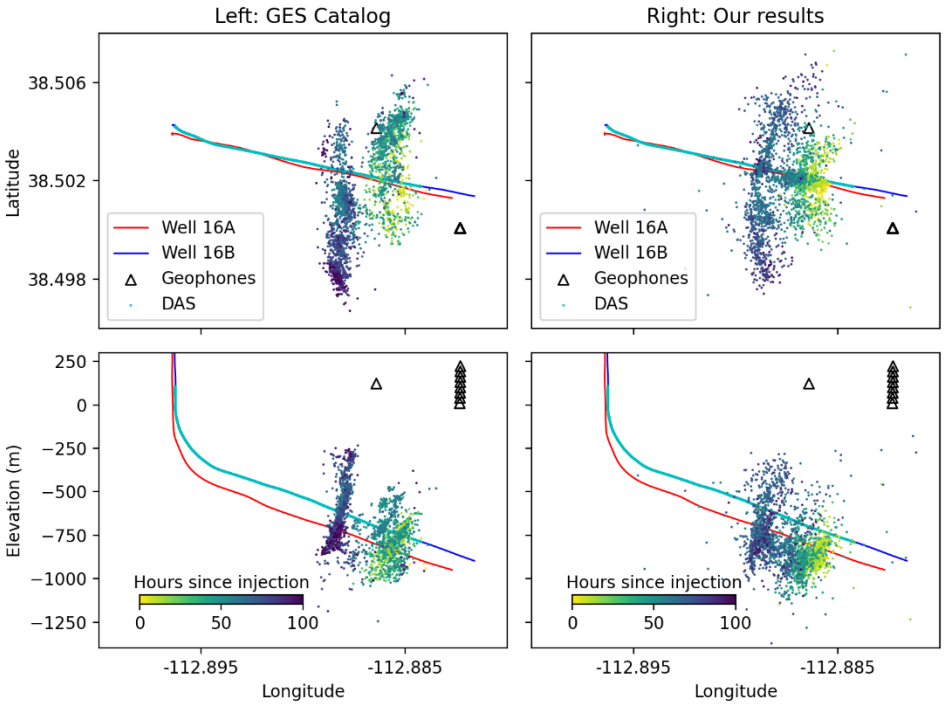

Figure 2: The comparison between the GES catalog (left) and the picks-based catalog (right) in this study.

Based on our bootstrapping analysis, the average location uncertainties in the longitudinal and vertical directions are ~26.2 m and ~25.4 m, respectively, while the average location uncertainty in the north-south direction is ~82 m, likely due to poorer coverage on the west and east sides. Some false picks may have been included during the location process, thereby affecting location accuracy. Mitigating false picks, which are mostly from noisy DAS recordings, would need to improve deep-learning model performance or add additional filtering steps during location.

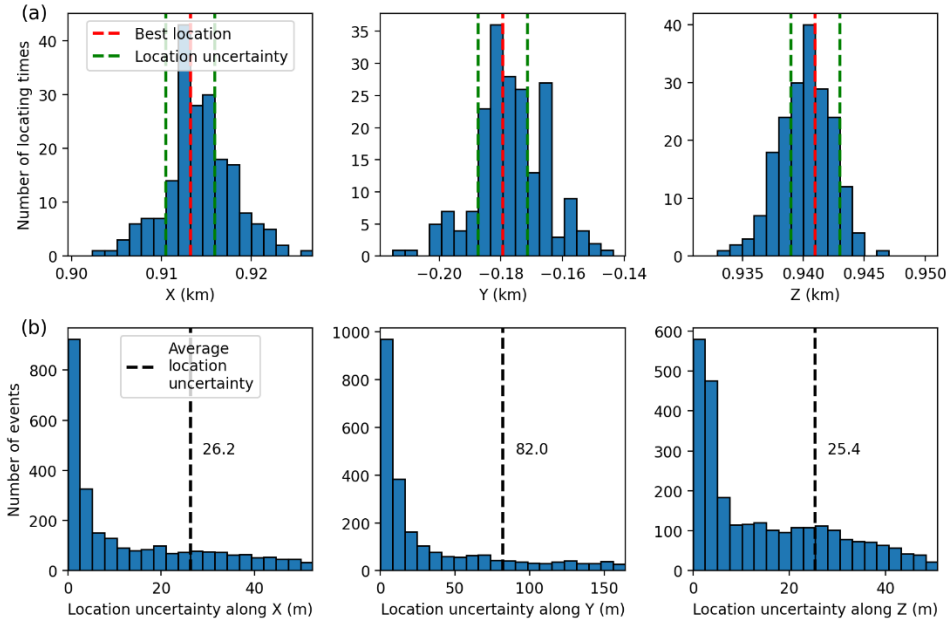

Figure 3: (a) For one example event, the distributions of locations by resampling 90% picks each time and repeating the locating step 200 times. (b) The distributions of location uncertainties for all the located events.

4.2 Microseismic Catalog from Waveform-Based Imaging

The 2024 FORGE dataset comprises 2680 microseismic events recorded by a hybrid network consisting of an eight-sensor three-component (3C) geophone array in borehole 78B-32 and a 1496-channel DAS array in borehole 16A(78)-32. Prior to analysis, a bandpass filter between 20 and 200 Hz was applied to both datasets to isolate the dominant signal energy. Following the STA/LTA transformation, the traces were time-shifted across the defined search grid, using theoretical travel times derived from the velocity model via the Eikonal equation. These time-shifted traces were then summed across all channels to generate a 'brightness' function, providing a quantitative measure of the wavefield's spatial coherency. This brightness volume was subsequently converted into a Probability Density Function (PDF), with the event location defined as the geometric median of the distribution.

The resulting PDFs demonstrate that integrating the 3C geophone array with the deviated fiber geometry (borehole 16A(78)-32) effectively breaks the DAS's inherent azimuthal symmetry. In contrast to the circular smearing observed in previous studies (Shimony & Lellouch, 2024), the sources are now tightly constrained. Across the full catalog, the method achieves an average spatial uncertainty of just 5 [m]. This represents a significant achievement of sub-grid resolution, providing precise locations well below the 40 [m] grid spacing used for the search. To optimize localization accuracy and constrain the velocity model, a systematic sensitivity analysis was performed on the $\frac{V_p}{V_s}$ ratio. Since the Source Scanning Algorithm relies on the coherent summation of P- and S-wave energy, an incorrect velocity ratio causes 'smearing' of the focal spot and degrades PDF coherency. We conducted a parameter sweep, testing a range of potential ratios while holding the P-wave velocity constant at a reference value of $V_p = 5530\ m/s$. The objective function exhibited a distinct maximum at a ratio of 1.715. This peak corresponds to the optimal constructive interference between the phases, ensuring that back-projected energy focuses on a consistent spatial location and origin time.

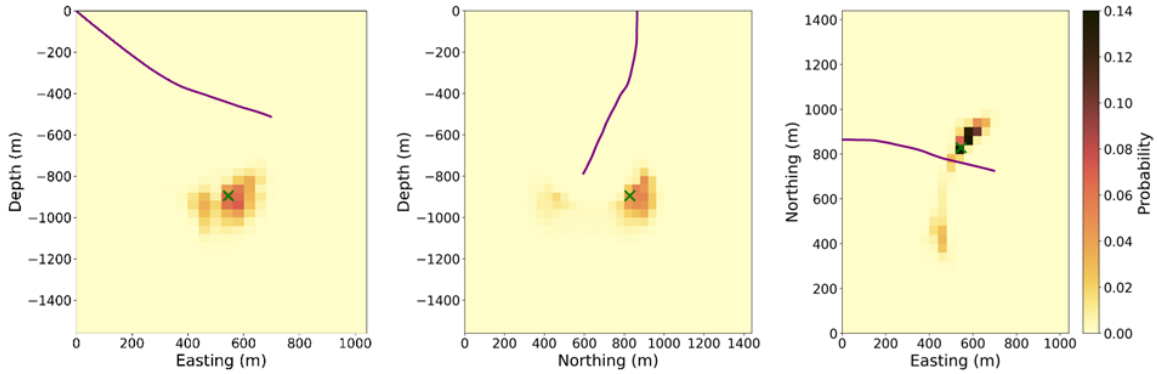

Figure 4: Probability map of a chosen event as a function of East-Depth (left), North-Depth (middle) and East-North (Right). The cylindrical symmetry inherent in the vertical DAS array is effectively broken by integrating geophone data. DAS fiber in purple and geometric median point in green.

Applying these optimized parameters to the full catalog of 2680 events generated a comprehensive three-dimensional map of the induced microseismicity. When projected onto 2D planes, the results shown in Figure 5 reveal the fracture network's mechanical response, characterized by a clear East-West orientation concentrated at approximately 700 [m] depth.

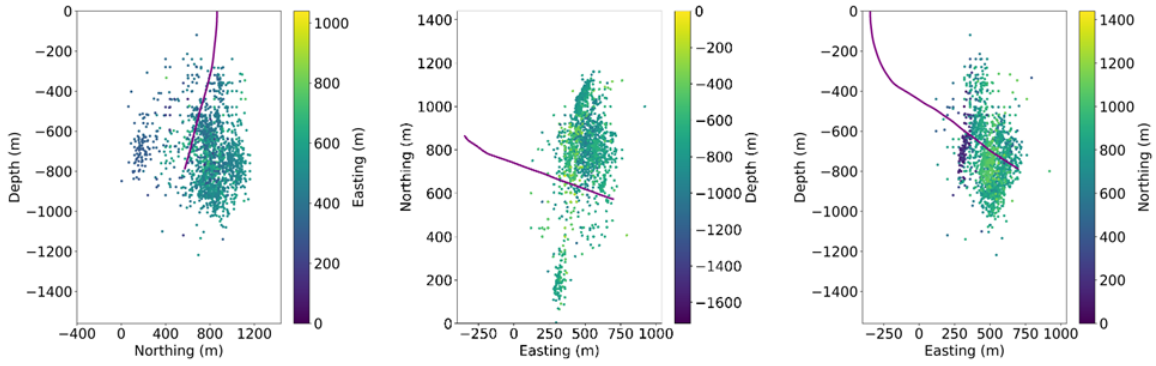

Figure 5: Estimated location of the 2680 events with the DAS fiber in purple. North-Depth view (left), Map view (middle), East-Depth view (Right).

4.3 Comparison of Microseismic Catalogs and Identified Faults

To evaluate the performance of different processing workflows, we compared microseismic catalogs generated using the Phase-Picking Event Location and Waveform-Based Source Imaging methods with the GES reference catalog. For each catalog, we applied an identical post-processing workflow (Zhang et al., 2025; Zhang & Dvory, 2025) to identify underlying fracture structures. Specifically, DBSCAN (Density-Based Spatial Clustering of Applications with Noise) was used to cluster spatially and temporally proximate events, followed by Principal Component Analysis (PCA) to fit planar surfaces to these clusters, representing potential fault structures.

Figure 6 presents the results derived from the Phase-Picking Event Location method. Panel A shows the three-dimensional spatial distribution of the microseismic events around the injection well 16A(78)-32 and the production well 16B(78)-32. The events exhibit clear clustering, allowing the DBSCAN and PCA workflow to resolve several distinct fault planes (shown as translucent colored surfaces). Panel B provides a map view of these identified hydraulic fractures (vertical) and faults (dips of approximately 60°). The major faults are oriented roughly parallel to the direction of the maximum horizontal stress (S_{Hmax} at N25°E), consistent with the geomechanical expectation that hydraulic fractures propagate in the direction of S_{Hmax}. The identified faults in this catalog exhibit relatively tight event clustering, defining clear planar features.

Figure 7 displays the results obtained using the Waveform-Based Source Imaging method. Similar to the phase-picking approach, Panel A visualizes the three-dimensional event locations and the resulting fitted fault planes, while Panel B shows the map view of these structures. Although this method successfully identifies the same major fracture zones and a similar orientation relative to S_{Hmax} as the phase-picking catalog, the spatial distribution of individual events appears more diffuse. Consequently, the fault planes derived from these cloudier clusters via PCA are less clearly defined than the phase-picking results.

Figure 8 shows the reference microseismic results provided by GES (Dyer et al., 2024). Panel A (3D view) and Panel B (map view) illustrate a high-density catalog in which microseismic events clearly delineate extensive and continuous fracture surfaces. A prominent fault with a dip of 77.15 ° is highlighted in purple in both views and is particularly well defined by intense event clustering, indicating a major stimulation zone. Compared to the catalogs generated using the Phase-Picking and Waveform-Based workflows, the GES results exhibit a slight azimuthal shift and appear less strictly parallel to S_{Hmax}.

A comparative analysis of the three figures reveals broad agreement in the macro-scale geometry of the stimulated reservoir. All three methods successfully delineate the primary fracture zones activated during stimulation, with the identified faults generally trending north-northeast. In the Phase-Picking Event Location (Figure 6) and Waveform-Based Source Imaging (Figure 7) catalogs, the identified faults are consistently oriented sub-parallel to S_{Hmax}. In contrast, the GES reference catalog (Figure 8) exhibits a slight azimuthal shift, appearing less strictly parallel to S_{Hmax}. Differences are also evident in the resolution of individual features. The Phase-Picking catalog (Figure 6) and the GES reference catalog (Figure 8) exhibit tighter spatial clustering of events, resulting in more clearly defined and apparently continuous fault planes after applying DBSCAN and PCA. In contrast, the Waveform-Based catalog (Figure 7) shows greater spatial scatter among individual events. While this method captures the overall location and orientation of the main structures, the increased scatter results in slightly less well-resolved fault-plane geometries. Notably, the Phase-Picking method resolves a high density of small-scale fault segments, providing a more scattered view of the fracture network that closely matches the structural complexity observed in the reference catalog.

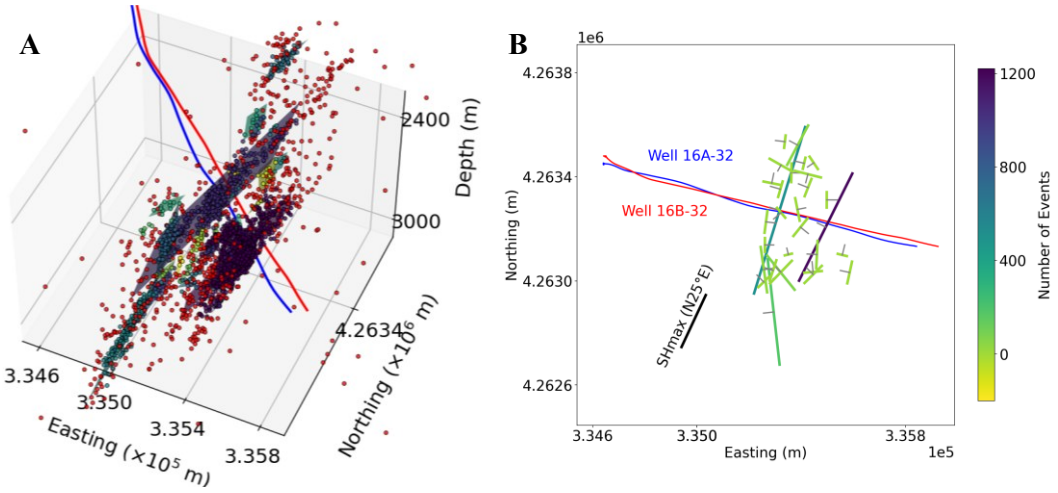

Figure 6: Three-dimensional (A) and map-view (B) representations of the identified faults based on the microseismic catalog obtained using the phase-picking event location method.

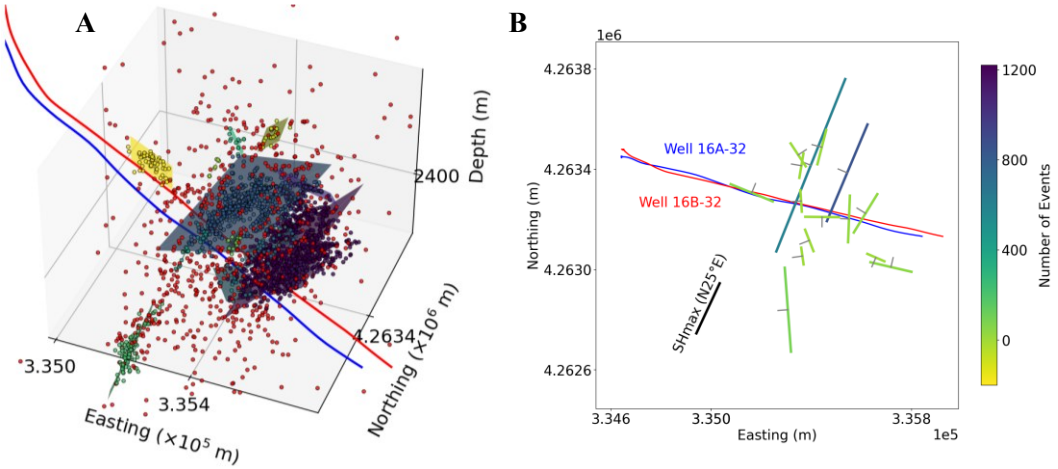

Figure 7: Three-dimensional (A) and map-view (B) representations of the identified faults based on the microseismic catalog derived from a waveform-based source imaging method.

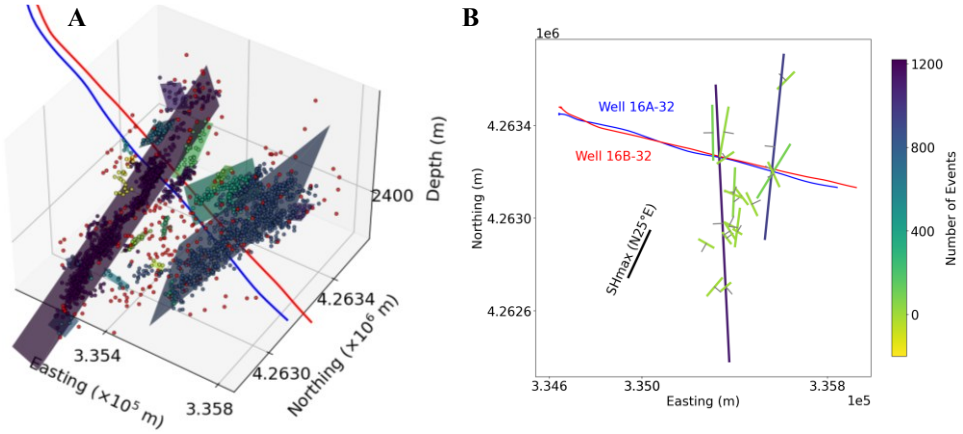

Figure 8: Three-dimensional (A) and map-view (B) representations of the identified faults based on the Geo Energy Suisse (GES) microseismic catalog.

5. CONCLUSIONS

This study demonstrates that integrating DAS and downhole geophone observations enables robust and high-resolution characterization of microseismicity and fracture geometry during hydraulic stimulation. A higher number of reliable phase picks yields more complete microseismic catalogs, particularly during stimulation along injection well 16A. However, DAS-dominated datasets remain sensitive to noise and source–receiver geometry, and DAS picks require careful filtering to mitigate false detections that can bias event locations, as observed during stimulation along the production well 16B.

The waveform-based source imaging workflow provides a powerful complement to traditional phase-picking approaches. By leveraging accurate receiver geometry, a calibrated velocity model, and grid-based back-projection, this method enables stable event localization even when individual DAS channels are noisy and phase picking is unreliable. The inclusion of three-component geophones is critical for breaking the intrinsic cylindrical symmetry of DAS arrays, while systematic velocity model optimization and probabilistic post-processing further enhance location robustness.

Despite employing a relatively coarse 40 m search grid to reduce computational cost, the proposed workflow achieves location uncertainties of approximately 5 m, reflecting the combined benefits of dense DAS spatial sampling and geophones' directional sensitivity. Comparative analysis shows broad agreement among the phase-picking, waveform-based, and reference (GES) catalogs in delineating the macro-scale geometry of the stimulated reservoir, while differences in fault-plane sharpness highlight the respective strengths of each approach.

These results suggest that hybrid workflows combining phase-picking and waveform-based imaging are well suited for real-time and near-real-time microseismic monitoring. Future developments should focus on adaptive DAS pick filtering, improved velocity model updating, and automated integration of multi-sensor data to further enhance resolution and reliability in complex reservoir environments.

ACKNOWLEDGEMENT

This project was supported by the Utah FORGE initiative, sponsored by the U.S. Department of Energy, under the project titled "Cutting-edge application of machine learning, geomechanics, and seismology for real-time decision-making tools during stimulation".

REFERENCES

Daley, T. M., Freifeld, B. M., Ajo-Franklin, J., Dou, S., Pevzner, R., Shulakova, V., et al. (2013). Field testing of fiber-optic distributed acoustic sensing (DAS) for subsurface seismic monitoring. *The Leading Edge*, *32*(6), 699–706. https://doi.org/10.1190/tle32060699.1

Dyer, B., Karvounis, D., & Bethmann, F. (2022). Utah FORGE: Seismic Event Catalogue from the April, 2022 Stimulation of Well 16A(78)-32. University of Utah Seismograph Stations. https://doi.org/10.15121/1879450

Dyer, B., Karvounis, D., Meier, P., Fiori, R., & Jaques, P. (2024). Utah FORGE: GES Well 16A(78)-32 and Well 16B(78)-32 Stimulation Seismic Event Catalogs. University of Utah Seismograph Stations. https://doi.org/10.15121/2455012

England, K. (2024). Utah FORGE: Wells 16A(78)-32 and 16B(78)-32 Stimulation Pressure and Circulation Data April, 2024. Energy and Geoscience Institute at the University of Utah. https://doi.org/10.15121/2371032

Folesky, J., Kummerow, J., Shapiro, S. A., Häring, M., & Asanuma, H. (2016). Rupture directivity of fluid-induced microseismic events: Observations from an enhanced geothermal system. *Journal of Geophysical Research: Solid Earth*, *121*(11), 8034–8047. https://doi.org/https://doi.org/10.1002/2016JB013078

Kao, H., & Shan, S.-J. (2004). The Source-Scanning Algorithm: mapping the distribution of seismic sources in time and space. *Geophysical Journal International*, *157*(2), 589–594. https://doi.org/https://doi.org/10.1111/j.1365-246X.2004.02276.x

Majer, E. L., Baria, R., Stark, M., Oates, S., Bommer, J., Smith, B., & Asanuma, H. (2007). Induced seismicity associated with Enhanced Geothermal Systems. *Geothermics*, *36*(3), 185–222. https://doi.org/https://doi.org/10.1016/j.geothermics.2007.03.003

McLennan, J. (2022). Utah FORGE: Well 16A(78)-32 Stimulation Data (April, 2022). Energy and Geoscience Institute at the University of Utah. https://doi.org/10.15121/1871203

Moore, J., McLennan, J., Allis, R., Pankow, K., Simmons, S., Podgorney, R., et al. (2019). The Utah Frontier Observatory for Research in Geothermal Energy (FORGE): an international laboratory for enhanced geothermal system technology development. In *44th Workshop on Geothermal Reservoir Engineering* (pp. 11–13). Stanford University.

Niemz, P., Pankow, K., Isken, M. P., Whidden, K., McLennan, J., & Moore, J. (2025). Mapping Fracture Zones with Nodal Geophone Patches: Insights from Induced Microseismicity During the 2024 Stimulations at Utah FORGE. *Seismological Research Letters*. https://doi.org/10.1785/0220240300

Perol, T., Gharbi, M., & Denolle, M. (2026). Convolutional neural network for earthquake detection and location. *Science Advances*, *4*(2), e1700578. https://doi.org/10.1126/sciadv.1700578

Shimony, E., & Lellouch, A. (2024). Microseismic Event Location with Dual Vertical DAS Arrays: Insights from the FORGE 2022 Stimulation. *Seismological Research Letters*, *95*(4), 2290–2304. https://doi.org/10.1785/0220230128

Stewart, S. W. (1977). Real-time detection and location of local seismic events in central California. *Bulletin of the Seismological Society of America*, *67*(2), 433–452. https://doi.org/10.1785/BSSA0670020433

Xiaoming, Z., & Dvory, N. Z. (2026). Integration of Maximum Magnitude Forecast and Ground Motion Prediction for Real-Time Seismic Hazard Assessment at Utah FORGE.

Zhan, Z. (2019). Distributed Acoustic Sensing Turns Fiber-Optic Cables into Sensitive Seismic Antennas. *Seismological Research Letters*, *91*(1), 1–15. https://doi.org/10.1785/0220190112

Zhang, M., Liu, M., Feng, T., Wang, R., & Zhu, W. (2022). LOC-FLOW: An end-to-end machine learning-based high-precision earthquake location workflow. *Seismological Society of America*, *93*(5), 2426–2438.

Zhang, X., Zhu, W., Salvage, R. O., & Dvory, N. Z. (2025). Deep Neural Network-Based Workflow for Accurate Seismic Catalog Generation from Low Resolution Seismic Data in Enhanced Geothermal System Operations. In *PROCEEDINGS, 50th Workshop on Geothermal Reservoir Engineering*. Stanford University.

Zhang, X. M., & Dvory, N. Z. (2025, June 8). Estimating Fault Slip Potential with CNN-Based Deep Learning: Integrating Mohr-Coulomb and Non-Linear Failure Criteria for Advanced Seismic Risk Assessment. *59th U.S. Rock Mechanics/Geomechanics Symposium*. https://doi.org/10.56952/ARMA-2025-0408

Zhu, W., & Beroza, G. C. (2019). PhaseNet: a deep-neural-network-based seismic arrival-time picking method. *Geophysical Journal International*, *216*(1), 261–273. https://doi.org/10.1093/gji/ggy423

Zhu, W., Rong, B., Jie, Y., & Wei, S. S. (2025). Robust Earthquake Location using Random Sample Consensus (RANSAC). *ArXiv Preprint ArXiv:2502.10933*.